

Discovery of Calcium-Metal Alloy Anodes for Reversible Ca-Ion Batteries

Zhenpeng Yao, Vinay I. Hegde, Alán Aspuru-Guzik,* and Chris Wolverton*

Ca-ion batteries (CIBs) show promise to achieve the high energy density required by emerging applications like electric vehicles because of their potentially improved capacities and high operating voltages. The development of CIBs is hindered by the failure of traditional graphite and calcium metal anodes due to the intercalation difficulty and the lack of efficient electrolytes. Recently, a high voltage (4.45 V) CIB cell using Sn as the anode has been reported to achieve a remarkable cyclability (>300 cycles). The calcination of Sn is observed to end at Ca_7Sn_6 , which is surprising, since higher Ca-content compounds are known (e.g., Ca_2Sn). Here, the Sn electrochemical calcination reaction process is investigated computationally and the reaction driving force as a function of Ca content is explored using density functional theory (DFT) calculations. This exploration allows the identification of threshold voltages which govern the limits of the calcination process. This information is then used to design a four-step screening strategy and high-throughput DFT is utilized to search for anode materials with higher properties. Many metalloids (Si, Sb, Ge), (post-)transition metals (Al, Pb, Cu, Cd, CdCu_2) are predicted to be promising inexpensive anode candidates and warrant further experimental investigations.

techniques with high energy density and low cost.^[1] Multivalent batteries, like Mg-ion,^[2] Ca-ion,^[3,4] and Al-ion batteries,^[5,6] have the potential to realize significantly improved capacities, compared to monovalent batteries (e.g., Li-ion batteries), due to more electrons carried per ion. Among them, Ca-ion batteries (CIB) have drawn special attention with merits besides the capacity enhancement: (1) Ca/ Ca^{2+} has a reduction potential (-2.87 V) only slightly higher than Li/ Li^+ (-3.04 V), yet much lower than Mg/ Mg^{2+} (-2.36 V) and Al/ Al^{3+} (-1.68 V), which provides CIB the prospect to function at voltages comparable with Li-ion batteries and much higher than the counterparts of Mg-ion and Al-ion batteries.^[7,8] (2) Ca is the fifth most abundant element in the earth's crust with an extensive global resource distribution, in contrast to lithium. (3) The kinetics of Ca-ion in solid electrodes are faster than Mg- and Al-ions due to reduced charge density.^[9–11]

1. Introduction

The usage of renewable energy, coupled with the growing application of electric vehicles (EVs), demand energy storage

The development of CIBs was originally pioneered by the study of Ca-ion electrochemical intercalations into layered transition metal oxides and sulfides.^[12] Subsequently, many efforts then were made to search for cathode materials which will tolerate a large amount of Ca-ions reversibly extracted/re-accommodated upon charge/discharge. Material systems including Prussian blue compounds,^[10,13,14] Chevrel phases,^[15,16] spinels,^[17–19] perovskites,^[20] layered transition metal (TM) sulfides,^[21] and iron phosphate,^[22] were suggested to be effective Ca-ion electrodes with the spinels and perovskites attracting extra attention because of their predicted high voltage (>3.5 V) and large theoretical capacities (>240 mAh g^{-1}) during discharge at room temperature.^[17–20] Distinct from these TM-based electrodes, a graphite cathode has been reported which functions via the (de-)intercalation of electrolyte salt anions ($\text{A}^- = \text{PF}_6^-, \text{ClO}_4^-,$ and so on) upon charge/discharge at remarkably high voltages (4.5–5.6 V)^[23,24] with a theoretical capacity as high as 372 mAh g^{-1} (corresponding to AC_6).^[24,25] Yet, the practical capacity of batteries based on this material suffers from a large degradation (≈ 90 mAh g^{-1}) as a result of the electrolyte decomposition under high voltage.^[24]

Unlike the continuous development of CIB cathode materials, studies focusing on anodes have been relatively scarce. Graphite-based CIB anodes have been shown to be problematic at room temperature due to difficulties related to the intercalation of calcium.^[26] The pursuit of a calcium metal

Dr. Z. Yao, Prof. A. Aspuru-Guzik
Department of Chemistry and Chemical Biology
Harvard University
12 Oxford Street, Cambridge, MA 02138, USA
E-mail: alan@aspuru.com

Dr. Z. Yao, V. I. Hegde, Prof. C. Wolverton
Department of Materials Science and Engineering
Northwestern University
2220 Campus Drive, Evanston, IL 60208, USA
E-mail: c-wolverton@northwestern.edu

Prof. A. Aspuru-Guzik
Department of Chemistry and Department of Computer Science
University of Toronto
Toronto, Ontario M5S 3H6, Canada

Prof. A. Aspuru-Guzik
Vector Institute for Artificial Intelligence
Toronto, Ontario M5S 1M1, Canada

Prof. A. Aspuru-Guzik
Canadian Institute for Advanced Research (CIFAR) Senior Fellow
Toronto, Ontario M5S 1M1, Canada

 The ORCID identification number(s) for the author(s) of this article can be found under <https://doi.org/10.1002/aenm.201802994>.

DOI: 10.1002/aenm.201802994

anode is currently hindered by the lack of an effective electrolyte to plate/strip calcium metal at room temperature^[3] in an adequate voltage window.^[4] Also, Ca²⁺ diffusion is observed to be extremely sluggish through the as-formed solid electrolyte interphase (SEI) between the calcium metal anode and the electrolyte.^[27,28] TM oxide (i.e., V₂O₅)^[29] based anodes have been shown to be effective at storing Ca-ions; however, the high calciation potential (≈ 2.8 V) of this material significantly reduces the overall output voltage of the whole cell.^[17]

Alloying-type anodes, widely studied for Li-ion batteries, show great promise for reversible CIBs. Using a Sn anode and graphite cathode, Wang et al.^[14] recently reported a high-voltage (4.45 V) CIB cell with a reasonable capacity of 85 mAh g and a remarkable cyclability (95% capacity retention in 350 cycles). Besides Sn, several metals and metalloids including Zn, Al, Si, Li, and Na have also been investigated for the use of alloying-type CIBs anodes with largely disparate capacities achieved.^[13,14,30,31] All of them except Na have been reported to mix with Ca in wide composition ranges, forming various intermetallic compounds.^[32] For instance, the highest Ca-content intermetallic compounds of Sn, Zn, and Li are Ca₂Sn,^[33] Ca₃Zn,^[34] and CaLi₂,^[35] with corresponding theoretical capacities calculated to be 903, 1366, and 3860 mAh g⁻¹. However, in experimental full-cell operations, the calciation of Sn ends at Ca₇Sn₆ with a theoretical capacity of 527 mAh g⁻¹ while the calciation of Zn and Li is even more truncated with very limited capacity observed.^[14] It is therefore important to examine the metal-calcium (M-Ca) reaction mechanisms during the electrochemical calciation and understand the variation of the calciation driving force as a function of Ca-ions accommodated. Furthermore, considering that Ca mixes with many metals and metalloids, forming a wide range of alloys and compounds,^[32] it is then of significant interest to explore the whole alloying space of M-Ca systems and discover novel active anode materials for improved electrochemical properties and cyclabilities.

First-principles density functional theory (DFT) calculations have been extensively used as compelling tools to study the battery materials by understanding the underlying mechanisms,^[36–41] exploring the kinetics during electrochemical reactions,^[42–45] and predicting novel high-performance electrode materials.^[46–49] Here in this work, we use DFT to investigate the Sn-Ca electrochemical alloy reaction process via constructing the ground-state Sn-Ca phase diagram and explore the reaction driving force evolution as a function of Ca-ion accommodated. We then identify the convex hull characteristics favored by large capacity alloy-type anodes and by comparison between our DFT calculations and electrochemical measurements of CIB cells, we define threshold calciation voltages which limit the extent of calciation reactions in real cells by examining the alloy reaction of Ca and Zn, Li, Na. Moreover, we design a four-step screening strategy and use high-throughput DFT calculations to explore all M-Ca alloying space to search for anode materials with higher energy density and constrained volume expansion. We predict that many metalloids (Si, Sb, Ge), (post-)transition metals (Al, Pb, Cu, Cd, CdCu₂, Ga, Bi, In, Tl, Hg), and noble metals (Ag, Au, Pt, Pd) are promising anode candidates. Our discoveries shed light on the design of high-performance reversible Ca-ion

batteries and provide predictions of new compounds awaiting experimental validation.

2. Results and Discussions

2.1. Sn-Ca Phase Diagram and the Electrochemical Sn-Ca Reactions

Phase diagrams represent the thermodynamic phase equilibria of multicomponent systems and provide useful information on the electrochemical reactions between phases. The ground-state convex hull represents the $T = 0$ K limit of the thermodynamic phase diagram and gives information about the ground-state stability of compounds in a given system. Experimental phase-diagram determination for a specific system can be time- and labor-consuming, while it can be significantly accelerated by calculating energies of all the known compounds in the corresponding chemical space using DFT.^[47] Here, we built M-Ca $T = 0$ K phase diagrams using structures with the lowest energy for each composition with M be metal/metalloids elements and their binary alloys. All the compounds were adopted from the Inorganic Crystal Structure Database (ICSD)^[50] and corresponding calculations were carried out under the framework of OQMD.^[51,52] Using these convex hulls, we analyze the electrochemical calciation process of Sn and examine the driving force variations to determine the calciation maximums for the Sn anode. Then we will validate our hypothesis in other typical systems including Zn, Li, and Na.

The calculated Sn-Ca convex hull is shown in **Figure 1A**, we are able to correctly identify all the known intermediate phases in the experimental phase diagram including CaSn₃, CaSn, Ca₇Sn₆, Ca₃₁Sn₂₀, Ca₃₆Sn₂₃, and Ca₂Sn as either on the hull or slightly (<10 meV/atom) above the hull.^[33] The calciation voltages corresponding to these phases declines from 0.99, 0.72, 0.59 to 0.53 V relative to Ca/Ca²⁺ (Figure 1B) while the volume expansion of the system per Ca accommodated increases from 7.4, 27.5, 27.6, 28.8 to 31.1 Å³ (Figure 1C). By comparison with experimental electrochemistry data, we can determine a cutoff for the allowed calciation driving force, below which the reaction will not proceed in practice. For instance, the experimental calciation of Sn ends at Ca₇Sn₆,^[14] and the calculated calciation voltage of the Sn-Ca system (Figure 1B) reaches a value of 0.53 V (relative to Ca/Ca²⁺) for Ca₇Sn₆. Hence, we use this comparison to hypothesize that the driving force for calciation of anodes should be no less than 0.53 V. We then validate the use of this driving force limit to determine the calciation extent of Zn, Li, and Na (and other metals), and compare with experimental measurements below. We also note that the shape of the convex hull can have a profound impact on the extent of calciation. The Sn-Ca convex hull features a relatively steep decreasing energy on the Sn-rich side. The fast decrease in formation energy with increasing Ca content corresponds to high calciation voltages and a large reaction driving force while the “length” (in Ca content) of this segment of the convex hull indicates a large amount of Ca ions react with the anode when the driving force is large. On the contrary, convex hulls which feature short or shallow decreasing segments on the Ca-poor side indicate a weak driving force, or small Ca capacity, and potentially point to a hasty end to calciation.

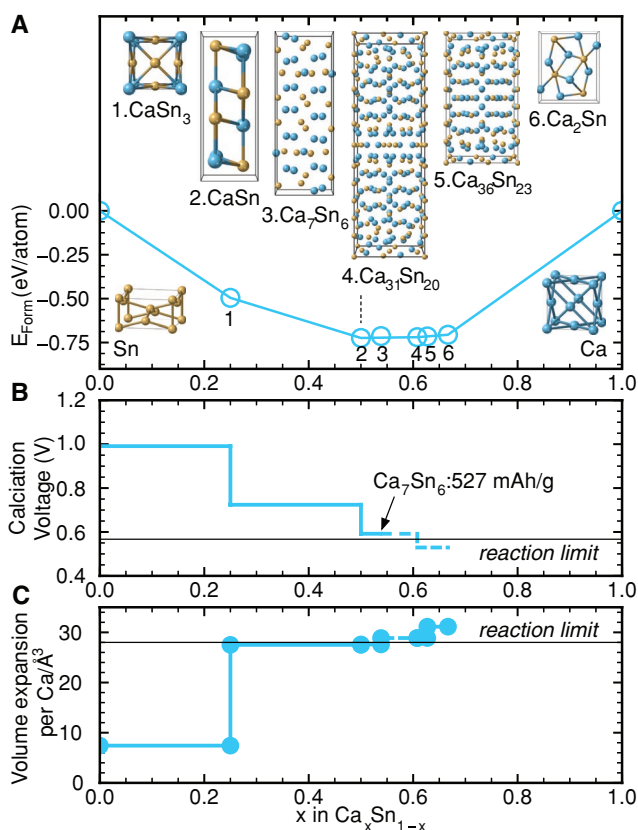


Figure 1. Electrochemical calcination process of Sn. A) Sn-Ca convex hull with all the known Sn-Ca intermetallic compounds predicted to be on or slightly (<10 meV/atom) above the convex hull. Structures for Sn, Ca, and all the intermetallic compound are shown in the insets. B) Corresponding calcination voltage profile during the calcination process of Sn. Experimentally observed calcination ends at Ca_7Sn_6 before the calcination voltage profile reaching the last plateau of 0.53 V,^[14] which can be seen as the threshold voltage of calcination. C) Calculated volume expansion per Ca as a function of calcination.

2.2. Ca-Zn, Li, Na Phase Diagrams and the Electrochemical Calcination Limits

Having determined a calcination voltage threshold in the Sn-Ca system, we next construct convex hulls in the Zn-Ca, Li-Ca, and Na-Ca systems, as shown in Figure 2A. The DFT calculations show nearly all experimentally observed intermediate compounds on the hull (except CaZn_3 which we exclude because its reported crystal structure exhibits partial occupancies). Na is reported to show no solubility in Ca with no intermetallic compound reported. As a simple test of the immiscibility and lack of compound formation in this system, we used Li_2Ca as a prototype and calculate the corresponding Na_2Ca energy. The phase is above the hull, consistent with the lack of observed compounds in this system. The Zn-Ca convex hull is asymmetric with low energies on the Zn-rich side, and formation energy of Ca_xZn rapidly decreases for small Ca concentrations ($0 < x < 0.33$). As a result, the calcination voltage quickly falls from 1.03 to 0.46 V (Figure 2B) in the same concentration range. If we apply the calcination voltage threshold derived from the Sn-Ca system (0.53 V) to the Zn-Ca system, then we

would predict its calcination should end at $x = 0.167$ (CaZn_5) and before $x = 0.33$ (CaZn_2), indicating a very limited calcination and capacity. These predictions are consistent with experimental observations,^[14] thus validating the use of the calcination voltage threshold. Zn also exhibits a larger volume expansion per Ca of 31.26 \AA^3 than Sn started at an early calcination step ($x = 0.167$) as shown in Figure 2C. For the calcination reaction of Li, because the convex hull is extremely shallow with very small (negative) formation energies, and thus a low calcination voltage of 0.03 V (Figure 2B). The Li-Ca calcination voltage is therefore significantly lower than the threshold calcination voltage value (0.53 V), and hence is predicted to exhibit very low reversible capacity, also in agreement with experimental observations,^[14] and therefore validating the use of the threshold. For Na, no stable intermediate phase with Ca is identified, which agrees with its poor calcination performance observed.^[14] In order to obtain a significant calcination capacity, one should search for M-Ca convex hulls with long and fast decreasing segments to the M-rich side to ensure large capacity with a high driving force. Having validated our strategy, we next use our threshold calcination voltage combined with high-throughput (HT) DFT of a large number of alloying-type anode calcination reactions to discover novel anodes with promising electrochemical properties.

2.3. HT-DFT Screening for High-Performance Novel Calcium Alloy Anodes

Ca forms alloys with many metals and metalloids.^[32] We use this fact, along with the threshold calcination voltage above to design a four-step screening strategy and apply it to search for the high electrochemical property anodes as shown in Figure 3. The four steps are: (i) The screening was initiated by identifying all the binary and ternary Ca intermetallic compounds from the ICSD.^[50] We exclude quaternary or higher order Ca alloys because of the potentially more complex mass transport (and hence sluggish kinetics) during their calcination and decalcination. In total, we identify unique 357 M-Ca compounds. (ii) We then examined all the Ca_xM compounds and checked the existence of counterparts with the same stoichiometry, but with Ca removed, that is, M. If both of them exist in the ICSD, the Ca_xM compound is then the potential calcination product of M where this latter compound is either simply a metal/metalloid element (e.g., Sn) or a binary intermetallic compound $\text{M}_a\text{M}'_b$ (e.g., CuAu). This screen results in a pool of 115 M-Ca systems with various number of calcination reactions. (iii) Next, we calculated calcination voltage profiles for calcination reactions of all 115 M-Ca systems as summarized in Figure 4. To determine the practical extent of the calcination reactions of each M-Ca system and also its maximum capacity, we apply threshold calcination voltages to all the M-Ca systems. Two factors were considered to define the threshold calcination voltages: calcium metal plating and the practical calcination limit (discussed above). Anodes calcination potentials lower than Ca/Ca^{2+} can experience calcium metal plating and possible dendrite formation, leading to possible short circuit and safety concerns. Therefore, we apply a first threshold calcination voltage of 0.1 V, which we term a relaxed criterion, to avoid

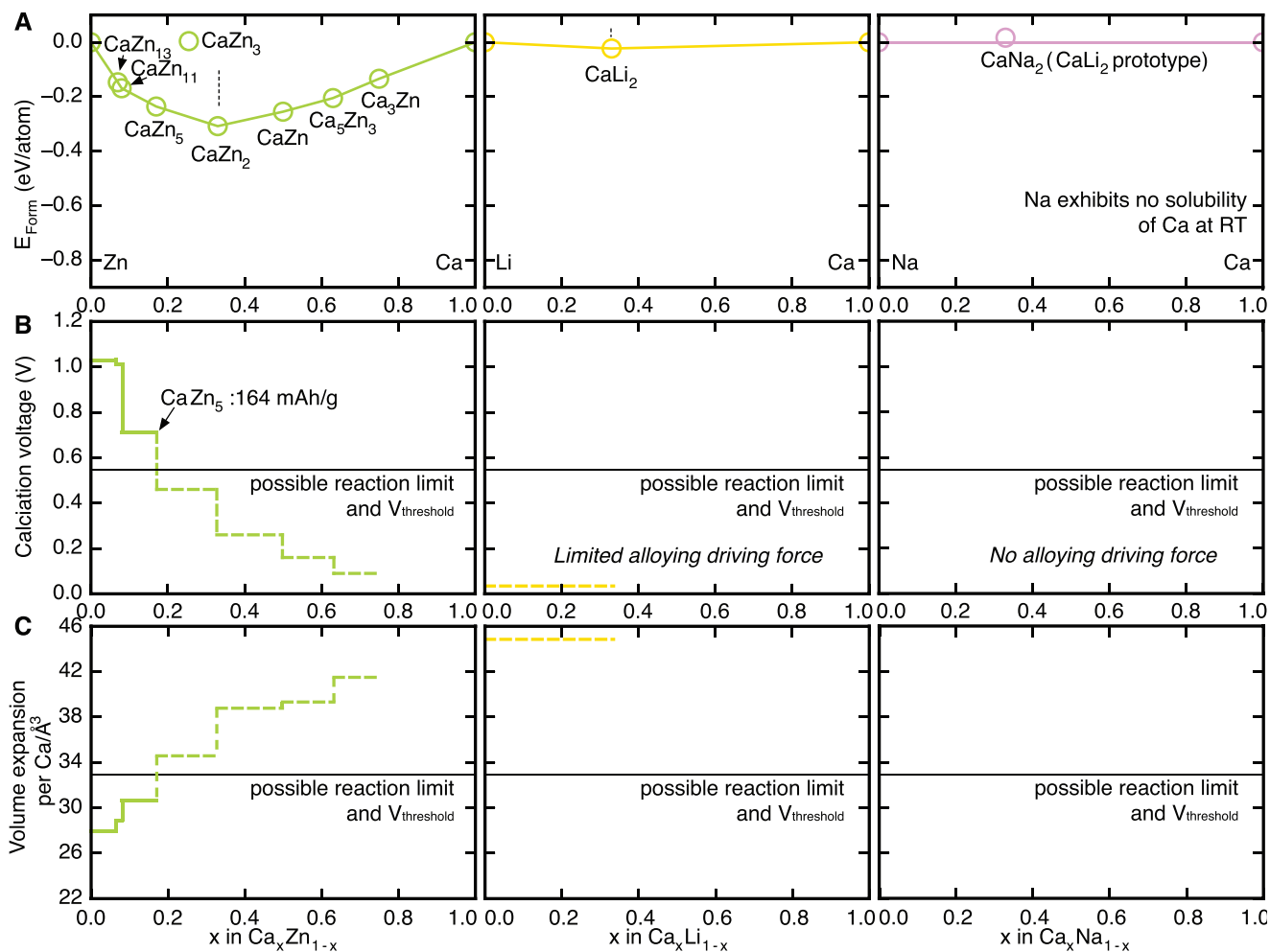


Figure 2. Electrochemical calcination processes of Zn, Li, Na and the determination of M-Ca alloy anode calcination threshold voltage. A) Zn-Ca, Li-Ca, Na-Ca convex hulls. B) Corresponding calcination voltage profiles during the calcination of Zn and Li. C) Calculated volume expansions per Ca upon calcination of Zn and Li. Compare with the Sn-Ca convex hull, the bottom of the Zn-Ca convex hull deviated to the Zn side with rapidly decreased formation energy in a small Ca concentration range indicating a fast calcination voltage declining and losing of reaction driving force. Similarly, the extremely shallow feature of the Li-Ca convex hull implying a low calcination voltage and inadequate reaction driving force, validating the observed significantly limited calcination capacity of Zn and Li.^[14] No stable intermetallic compound is identified for the Na-Ca convex hull, reflecting the fact of no solubility of Ca in Na.

calcium plating and potential failure of the cell. Meanwhile, we also apply a second threshold calcination voltage of 0.53 V, obtained by determining the practical Sn calcination maximum as discussed above. The calcination driving force requirements for M-Ca systems could be different from Sn-Ca (although we validated this strategy above for Zn-Ca, Na-Ca, and Li-Ca systems), yielding some uncertainty in the predictions. Hence, we use both thresholds with 0.53 V serving as the restrictive criterion and the 0.1 V serving as the relaxed criterion. We repeated each screening calculation with both thresholds to illustrate the changes that could occur with a range of calcination thresholds. Then two capacity maximums (C_{max}) of each M-Ca system are determined. (iv) For the two datasets obtained with different threshold calcination voltages, we estimated their output voltages refer to the $V_{cathode}$ assumed, volume expansions, specific energies, and energy densities and rank them using their maximum capacities and energy densities.

Cyclabilities of alloying-type anodes are usually deteriorated by a large volume expansion due to ion insertions as we learned from the Li-ion batteries^[53] and M-Ca systems with lower volume expansions are then favored. We then screen for M-Ca systems with a higher energy density than Sn, yielding a list of the most promising anode candidates.

2.3.1. Anode Candidates Obtained with the Relaxed Calcination Voltage Criterion

Metalloids (Si, Ge, As, Sb): Our screening strategy identifies metalloids including Si, Ge, As, and Sb as compelling anode materials with high specific energies and remarkably constrained volume expansions as shown in **Figure 5**. Among them, Si exhibits the highest gravimetric capacity (3817 mAh g⁻¹) and specific energy (17 732 Wh kg⁻¹, calculated with graphite

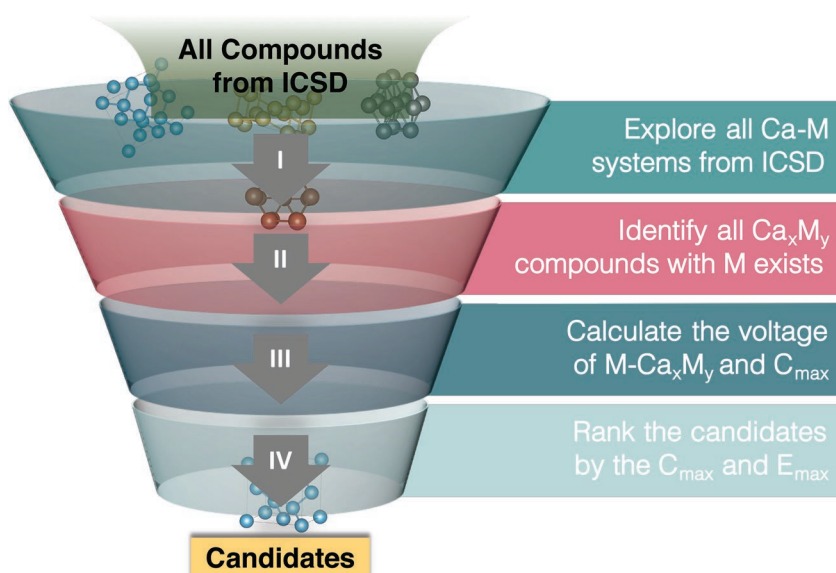


Figure 3. Screening strategy for the search of calcium-metal alloy anodes. We proceeded the high-throughput screening following a four-step strategy. Started with all the compounds in the Inorganic Crystal Structure Database (ICSD), we identify the M-Ca alloys for which the M also exists in the ICSD with M can be metal elements and other alloys. Then we calculate the reaction voltage profiles for each M-Ca system and determine its maximum capacity C_{\max} . Finally, we evaluate the energy densities E_{\max} corresponding to C_{\max} of all the systems using their output voltage, rank them based on their E_{\max} values, and select the ones with highest energy densities as our top candidates.

cathode usage assumed as discussed in Capacity and Energy Density Calculations section) in this study by taking as many as two Ca. These attributes are significantly larger than the analogous properties of Sn (903 mAh g⁻¹, 4036 Wh kg⁻¹) when the lower threshold calcination voltage is applied. The average calcination voltage for the Si anode, 0.35 V, is modest. Meanwhile, its maximum volume expansion is 31.89 Å³ per Ca and is comparable to Sn (31.13 Å³ per Ca). Ge, As and Sb can also take a maximum amount of two Ca per M when the low threshold calcination voltage was applied, and their heavier masses make their gravimetric capacities (1476, 1431, 880 mAh g⁻¹) and

specific energies (6685, 6085, 3809 Wh kg⁻¹) slightly lower than Si, yet still comparable or higher than Sn. Moreover, Ge, As, and Sb exhibit much lower volume expansion maximums than Sn: 31.06, 30.93, and 29.66 Å³ per Ca.

Post-Transition metals (Ga, Al, In, Tl, Pb, Hg, Cd, Zn): Post-transition metals contain candidates among which several have been investigated experimentally as anodes of CIBs such as Sn, Al, and Zn. Boron-group metals including Ga and Al exhibit attractive properties as alloy anodes for CIB because of their second and third highest specific energies (9355, 8702 Wh kg⁻¹) predicted in this study (following Si) as well as outstanding gravimetric and volumetric capacities. Moreover, Al has a potentially low cost making it appealing for practical use in CIBs. The other two boron-group candidates (i.e., In and Tl) can also accommodate significant amounts of Ca (Ca₃In, Ca₃Tl) and exhibit high volumetric properties (Table 1) with volume expansions much lower than Ga and Al. Similar to In and Tl, Pb can accommodate three Ca per atom upon calcination with higher volumetric properties than Sn and the lowest volume expansion predicted in

this study of 28.10 Å³ per Ca, indicating the possibility of superior cycling performance than other candidates. Hg has been tried as liquid-state anode for CIB because of its low melting point, however, there are many intermetallic compounds in the Ca-Hg system that are stable at room temperature.^[54] Thus to use Hg as an anode in a practical CIB, one could start with the lowest Ca-content compound of CaHg₃^[54] and control the extent of decalcination to avoid the formation of liquid Hg metal. CaHg₃ has slightly lower gravimetric properties than Sn yet much higher volumetric capacity (7662 mAh mL⁻¹) and energy density (37 390 Wh L⁻¹). Cd has been widely used

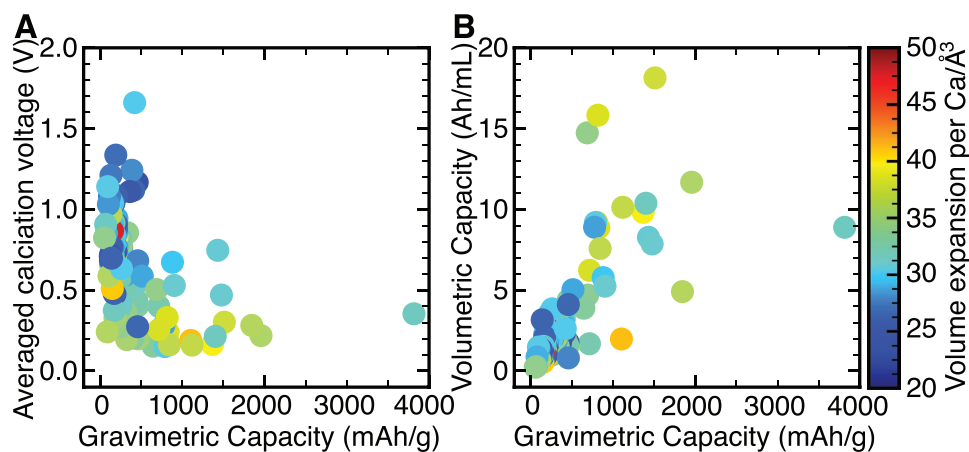


Figure 4. Summary of the identified M-Ca systems and corresponding properties. A) Averaged calcination voltages and gravimetric capacities and B) volumetric capacities of all the 115 M-Ca systems. The color of each marker indicates the volume expansion per Ca corresponding to the final product of specific M-Ca system.

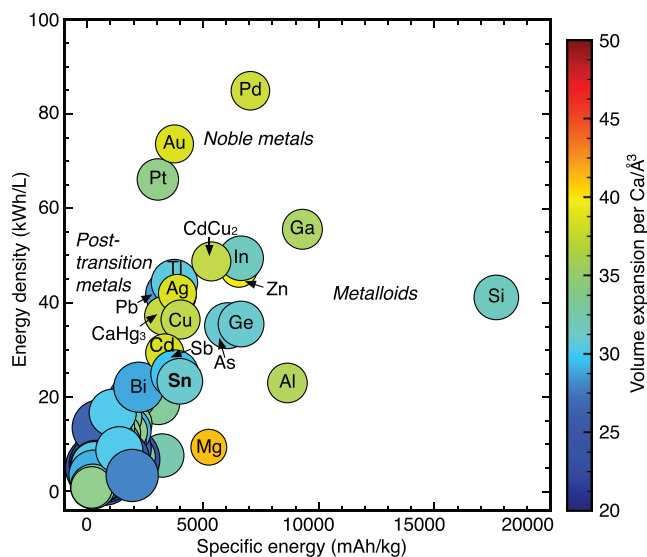


Figure 5. HT-DFT screening results for high-performance M-Ca anodes with relaxed voltage constraint. We performed computational screening for M-Ca alloy-type anode materials. Candidates are systems with energy densities and specific energies (calculated with graphite cathode usage assumed as discussed in Capacity and Energy Density Calculations section) higher than the counterparts of Sn. The color (and size) of each marker indicates the volume expansion (inverted trend for size) per Ca. Our top candidates are metalloids (Si, Ge, As, Sb), post-transition metals (Ga, Al, In, Tl, Pb, Hg, Cd), transition metals (Cu, CdCu₂), and noble metals (Pd, Au, Pt, Ag).

in rechargeable NiCd batteries and here, we predict it to be a promising candidate for CIB with higher volumetric capacity (6227 mAh mL⁻¹) and energy density (29 542 Wh L⁻¹) than Sn. Zn as an anode has been reported to fail^[14] because of the rapid decreasing driving force in a very limited calcination concentration range.

Transition Metal and Alloys (Cu, CdCu₂): Cu and CdCu₂ feature improved energy densities compared to Sn (4080, 5414 Wh kg⁻¹). Meanwhile, Cu and its alloys have remarkable electrical conductivity which is a promising attribute for potential high-rate electrodes. In addition, their competitive costs which make them attractive for further experimental validations.

Noble Metals (Pd, Au, Pt, Ag): Noble metal candidates (Pd, Au, Pt) exhibit the highest volumetric capacities (18 141, 15 830, 14 738 mAh mL⁻¹) and energy densities (85 225, 73 911, 66 261 Wh L⁻¹) in this study by taking significant amount of Ca per metal (Ca₃Pd, Ca₃Au, Ca₃Pt₂). The calcination of Pd, Au, and Pt also occurs at quite high calcination voltages for a large concentration range (Table S1, Supporting Information) which ensure large reaction driving forces. Ag also shows improved volumetric properties compared to Sn at relatively lower potential (0.24 V). Moreover, the noble metals' superior electrical conductivity and chemical stability against corrosion make them attractive candidates to be explored for CIB anodes. Their relatively high cost (except possibly Ag) may impair their large-scale applications yet their superb predicted properties make them worthy of scientific exploration.

Table 1. Candidates for high-performance M-Ca alloy-type anodes with relaxed voltage constraint ($V_{\text{threshold}} = 0.1$ V). For each candidate system, we show the reactant, final product, averaged voltage, gravimetric capacity, volumetric capacity, energy density, specific energy, and volume expansion maximum.

Candidates and reactions	Averaged calcination voltage [V]	Gravimetric capacity [mAh g ⁻¹]	Volumetric capacity [mAh mL ⁻¹]	Energy density [Wh L ⁻¹]	Specific energy [Wh kg ⁻¹]	Volume expansion per Ca [Å ³]	Volume expansion [%]
Si + 2Ca → Ca ₂ Si	0.35	3817	8892	41 310	17 732	31.89	318.64
Ga + 28/11Ca → 1/11Ca ₂₈ Ga ₁₁	0.22	1957	11 680	55 842	9355	36.12	474.07
Al + 13/14Ca → 1/14Ca ₁₃ Al ₁₄	0.28	1845	4910	23 167	8702	36.47	201.22
Pd + 3Ca → Ca ₃ Pd	0.30	1511	18 141	85 225	7098	37.75	769.50
In + 3Ca → Ca ₃ In	0.21	1400	10 381	49 682	6702	31.89	372.00
Ge + 2Ca → Ca ₂ Ge	0.47	1476	7864	35 622	6685	31.06	274.47
Zn + 5/3Ca → 1/3Ca ₅ Zn ₃	0.16	1366	9816	47 472	6607	39.78	438.78
As + 2Ca → Ca ₂ As	0.75	1431	8271	35 176	6085	30.93	287.48
CdCu ₂ + 5Ca → Ca ₅ CdCu ₂	0.16	1119	10 130	49 030	5414	37.14	422.89
Cu + Ca → CaCu	0.16	843	7581	36 676	4080	37.10	315.98
Ag + 5/3Ca → 1/3Ca ₅ Ag ₃	0.24	828	8866	42 209	3943	38.47	383.18
Sb + 2Ca → Ca ₂ Sb	0.67	880	5778	25 000	3809	29.66	192.56
Au + 3Ca → Ca ₃ Au	0.33	816	15 830	73 911	3811	38.42	683.38
Tl + 3Ca → Ca ₃ Tl	0.15	787	9185	44 536	3815	30.62	316.01
Pb + 3Ca → Ca ₃ Pb	0.28	776	8897	41 965	3660	28.10	280.85
Cd + 3/2Ca → 1/2Ca ₃ Cd ₂	0.26	715	6227	29 542	3393	38.22	267.43
Pt + 5/2Ca → 1/2Ca ₅ Pt ₂	0.50	687	14 738	66 261	3088	34.62	573.37
1/3CaHg ₃ + 8/3Ca → Ca ₃ Hg	0.12	668	7662	37 390	3259	37.25	291.07
Sn + 2Ca → Ca ₂ Sn	0.53	903	5249	23 465	4036	31.13	183.64

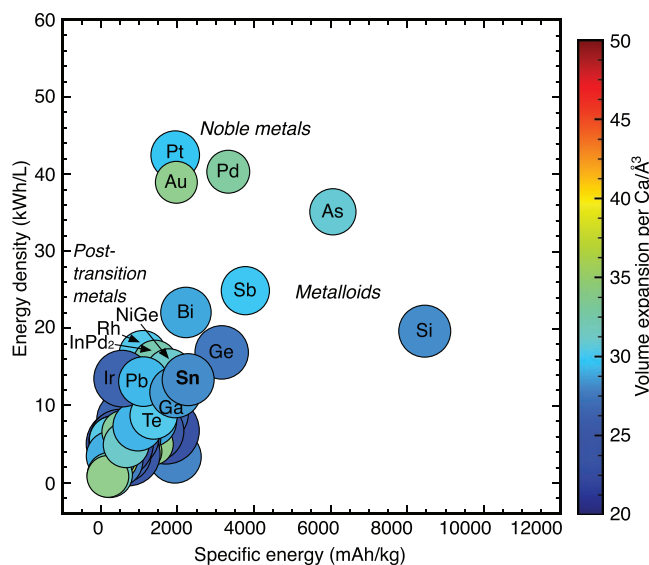


Figure 6. HT-DFT screening results for high-performance M-Ca anodes with restrictive voltage constraint. We performed computational screening for M-Ca alloy-type anode materials. Candidates are systems with energy densities and specific energies (calculated with graphite cathode usage assumed as discussed in Capacity and Energy Density Calculations section) higher than the counterparts of Sn. The color (and size) of each marker indicates the volume expansion (inversed trend for size) per Ca. Our top candidates are metalloids (Si, As, Sb, Ge), post-transition metals (Bi, As, Sb, Ge), and noble metals (Pt, Pd, Au).

2.3.2. Anode Candidates Obtained with the Restrictive Calcination Voltage Criterion

Metalloids (Si, As, Sb, Ge): Metalloids are still the strongest anode candidates (**Figure 6**) even with the strict calcination voltage threshold criterion and concomitant truncated calcination reaction (**Table 2** and **Table S2**, Supporting Information). Si, As, Sb, and Ge exhibit highest gravimetric properties (gravimetric capacity: 1908, 1431, 880, 738 mAh g⁻¹; specific energy: 8492, 6085, 3809, 3193 Wh kg⁻¹) which are significantly higher than Sn (527 mAh g⁻¹, 2321 Wh kg⁻¹) while Si and Ge also show competitive volume expansions (27.6, 26.9 Å³ per Ca) compared

to Sn (27.59 Å³ per Ca). Si and Sb alloy-type anodes have also been extensively investigated in the Li-ion battery field, and their predicted properties suggest further experimental investigation of these anodes in CIB is warranted.

Post-Transition Metals (Bi): Most post-transition metals which form alloys with Ca as discussed in the previous section experience lower calcination voltage compared with the restrictive voltage threshold. Bi emerges under the restrictive voltage threshold to be strong candidate CIB anode because of its comparable gravimetric properties with Sn yet much improved volumetric properties (5031 mAh mL⁻¹, 22 200 Wh L⁻¹) and constrained volume expansion of 28.37 Å³ per Ca.

Noble Metals (Pt, Pd, Au): The noble metals, Pd, Au, and Pt, have relatively high calcination voltages over wide calcination reaction extents (Ca₃Pd₂, Ca₅Au₃, Ca₅Pt₃) and large energy densities (40 445, 39 066, 42 533 Wh L⁻¹) with the strict criterion of 0.53 V. Their large volume expansions also get significantly relieved after the calcination reaction truncations (**Table S2**, Supporting Information). Noble metals are still strong candidates for CIBs and scientific exploration.

3. Conclusions

In this study, we investigate the Sn-Ca electrochemical alloy reaction process via constructing the Sn-Ca *T* = 0 K phase diagram and explore the reaction driving force evolution as a function of Ca-ion content accommodated. We identify the convex hull characteristics favored by large capacity alloy-type anodes which are then validated by Zn-Ca, Li-Ca, and Na-Ca systems and define threshold voltages to explain and determine the calcination reaction extent. Two threshold voltages are then put forward corresponding to the restrictive and relaxed criterions. The former threshold is based on the observed calcination behavior of Sn, and the latter threshold is based on avoiding Ca metal plating and the possibility of dendrite formation. We design a four-step screening strategy based on voltage thresholds and use high-throughput DFT calculations to explore all M-Ca alloying spaces to search for anode materials with properties superior to the recently reported Sn anodes. We predict that many metalloids (Si, Sb, Ge), (post-)transition metals

Table 2. Candidates for high-performance M-Ca alloy-type anodes with restrictive voltage constraint ($V_{\text{threshold}} = 0.53$ V). For each candidate system, we show the reactant, final product, averaged voltage, gravimetric capacity, volumetric capacity, energy density, specific energy, and volume expansion maximum.

Candidates and reactions	Averaged calcination voltage [V]	Gravimetric capacity [mAh g ⁻¹]	Volumetric capacity [mAh mL ⁻¹]	Energy density [Wh L ⁻¹]	Specific energy [Wh kg ⁻¹]	Volume expansion per Ca [Å ³]	Volume expansion [%]
Si + Ca → CaSi	0.55	1908	4446	19 784	8492	27.60	137.85
As + 2Ca → Ca ₂ As	0.75	1431	8271	35 176	6085	30.93	287.48
Sb + 2Ca → Ca ₂ Sb	0.67	880	5778	25 000	3809	29.66	192.56
Pd + 3/2Ca → 1/2Ca ₃ Pd ₂	0.54	755	9070	40 445	3368	33.50	341.44
Ge + Ca → CaGe	0.67	738	3932	17 013	3193	26.90	118.83
Bi + 2Ca → Ca ₂ Bi	0.59	513	5031	22 200	2264	28.37	160.35
Pt + 5/3Ca → 1/3Ca ₅ Pt ₃	0.67	458	9825	42 533	1982	29.40	324.58
Au + 5/3Ca → 1/3Ca ₅ Au ₃	0.56	454	8795	39 066	2014	34.41	340.43
Sn + 7/6Ca → 1/6Ca ₇ Sn ₆	0.59	527	3062	13 496	2321	27.59	94.94

(Al, Pb, Cu, Cd, CdCu₂, Ga, Bi, In, Tl, Hg), and noble metals (Ag, Au, Pt, Pd) are promising anode candidates and worthy of further experimental validation. Our theoretical findings provide insights into the electrochemical calciation reaction process of alloy-type CIB anodes and could help in designing the reversible high-energy density CIB anode materials.

4. Computational Methods

First-Principles DFT Calculations: All the first-principles calculations were performed via the Vienna Ab Initio Simulation Package (VASP)^[55–58] within the projector augmented wave (PAW) formalism^[59] and the Perdew–Burke–Ernzerhof (PBE) approximation^[60] to the exchange–correlation potential was employed. A plane wave basis with a cutoff energy of 520 eV and Γ -centered k -meshes with a density of 8000 k -points per reciprocal atom were used. All the calculations reported in this study were conducted under the framework of the Open Quantum Materials Database (OQMD).^[51,52]

Calculation Voltage V of M-Ca Anode: The averaged M-Ca electrochemical alloy reaction voltages (calciation voltage, relative to Ca/Ca²⁺) were evaluated by calculating the reaction free energy per Ca added/removed, as shown in Equation (1)^[61,62]

$$V = \frac{\Delta G_f}{2F\Delta N_{Ca}} \quad (1)$$

where F is the Faraday constant, ΔN_{Ca} is the amount of Ca added/removed, 2 is the amount of charges carried per single Ca, and ΔG_f is the molar free energy change during the reaction. Assuming that the calciation proceeds through a two-phase reaction between Ca_xM and M: $M + xCa \rightarrow Ca_xM$, ΔG_f can be approximated by the total internal energy changes from DFT calculations (0 K)

$$\Delta E = E(Ca_xM) - E(M) - xE(Ca_{metal}) \quad (2)$$

where $E(Ca_xM)$ and $E(M)$ are the DFT energies at the respective compositions. Entropic contributions were neglected and the reaction voltage profiles therefore will follow the $T = 0$ K ground-state convex hull and consist of a series of constant voltage steps along the two-phase regions of the convex hull, separated by discontinuities indicating the single-phase compounds on the hull. It is noteworthy that electrochemical M-Ca reactions do not necessarily proceed through two-phase reactions in practice. Thus, the calculated $T = 0$ K voltage profiles should be viewed as an approximation to the actual voltage profiles.^[63,64] The voltage drops in the profile become more rounded at finite temperatures (e.g., room temperature), due to finite temperature effects.^[62]

Output Voltage V_{output} of CIBs Using the M-Ca Anode: During the discharge of CIBs, the M-Ca alloy anode, which is the focus of this study, experiences a decalciation reaction (corresponding voltage: $-V$) while the corresponding cathode experiences a calciation reaction (corresponding voltage: $V_{cathode}$). Upon charging, the reverse reactions occur. The output voltage of a complete CIB cell containing both cathode and anode upon discharge can then be defined as follows

$$V_{output} = V_{cathode} - V \quad (3)$$

where the anode voltage V can be calculated using Equation (1). To calculate the output voltage and then evaluate the energy densities of CIBs using anodes discovered in this study, a value of $V_{cathode} = 5.04$ V (vs Ca/Ca²⁺) is assumed, which is obtained as the addition of experiment overall output voltage 4.45 V^[4] (vs Sn anode) and DFT calculated averaged Sn anode voltage (0.59 V, till Ca₇Sn₆, vs Ca/Ca²⁺).

Anodes with lower calciation voltage V to maximize the V_{output} of CIB were favored, yet V should not be too low to ensure enough driving force for the reversed calciation reaction to happen on charge.

Volume Expansion Evaluations: The volume expansion was computed upon the calciation of M via calculating the volume change per Ca added as shown in Equation (4)

$$U = \frac{u_{Ca_xM} - u_M}{x} \quad (4)$$

where u_{Ca_xM} and u_M are the volumes of Ca_xM and M, respectively, and x is the amount of Ca.

The relative volume expansion upon the calciation of M is also calculated as follows in Equation (5)

$$U_R = \frac{u_{Ca_xM} - u_M}{u_M} \times 100\% \quad (5)$$

Capacity and Energy Density Calculations: The gravimetric and volumetric capacity of M-Ca alloy anode corresponding to a given voltage plateau (a given two-phase reaction) can be calculated according to Equations (6) and (7)

$$C_g(V) = \frac{2\Delta N_{Ca}(V)F}{m_M} \quad (6)$$

$$C_u(V) = \frac{2\Delta N_{Ca}(V)F}{u_M} \quad (7)$$

where F is the Faraday constant, $\Delta N_{Ca}(V)$ is the amount of Ca added/removed corresponding to the voltage plateau, 2 is the amount of charge carried per single Ca, m_M and u_M are the mass and volume of M, respectively.

The energy density $E_g(V)$ and specific energy $E_u(V)$ of the CIBs using the M-Ca alloy anode can then be calculated by integrating the volumetric capacity $C_g(V)$ and gravimetric capacity $C_u(V)$ as a function of output voltage V_{output} as shown in Equations (8) and (9)

$$E_g(V) = \int_{V_0}^{V_0} C_g(V_{cathode} - V') dV' \quad (8)$$

$$E_u(V) = \int_{V_0}^{V_0} C_u(V_{cathode} - V') dV' \quad (9)$$

where V_0 is the lower limit of M calciation voltage profile.

Supporting Information

Supporting Information is available from the Wiley Online Library or from the author.

Acknowledgements

Z.Y. (conceived the idea, DFT calculations, and analysis of results) and A.A.-G. (leadership of project) were supported as part of the Nanoporous Materials Genome Center by the U.S. Department of Energy, Office of Science, Office of Basic Energy Sciences under Award No. DE-SC0008688. C.W. (leadership of project) was supported as part of the Center for Electrochemical Energy Science (CEES), an Energy Frontier Research Center funded by the U.S. Department of Energy, Office of the Science, Basic Energy Science under Award No. DE-AC02-06CH11357. V.I.H. (high-throughput workflows) acknowledges support from the Center for Hierarchical Materials Design (CHiMaD) and from the U.S. Department of Commerce, National Institute of Standards and Technology under Award No. 70NANB14H012. The authors gratefully acknowledge the computing resources from: (1) the National Energy Research Scientific Computing Center, a DOE Office of Science User Facility supported by the Office of Science of the U.S. Department of Energy under Contract

No. DE-AC02-05CH11231. (2) Blues, a high-performance computing cluster operated by the Laboratory Computing Resource Center at Argonne National Laboratory. Z.Y. conceived the overall project and DFT calculation of ground-state structure prediction, structural pathway, voltage and energy density. C.W. provided overall direction and advice for project, and analyzed the results. V.I.H. performed high-throughput calculation of doping options. A.A-G. provided feedback for the project. All data needed to evaluate the conclusions in the paper are present in the paper and/or the Supporting Information. Additional data related to this paper may be requested from the authors.

Conflict of Interest

The authors declare no conflict of interest.

Keywords

alloy-type electrodes, calcium-ion batteries, high-energy-density electrodes, high-throughput screening

Received: September 26, 2018

Revised: December 17, 2018

Published online:

-
- [1] D. Larcher, J.-M. Tarascon, *Nat. Chem.* **2015**, *7*, 19.
- [2] D. Aurbach, Z. Lu, A. Schechter, Y. Gofer, H. Gizbar, R. Turgeman, Y. Cohen, M. Moshkovich, E. Levi, *Nature* **2000**, *407*, 724.
- [3] A. Ponrouch, C. Frontera, F. Bardé, M. R. Palacín, *Nat. Mater.* **2016**, *15*, 169.
- [4] D. Wang, X. Gao, Y. Chen, L. Jin, C. Kuss, P. G. Bruce, *Nat. Mater.* **2017**, *17*, 16.
- [5] M.-C. Lin, M. Gong, B. Lu, Y. Wu, D.-Y. Wang, M. Guan, M. Angell, C. Chen, J. Yang, B.-J. Hwang, H. Dai, *Nature* **2015**, *520*, 324.
- [6] D.-Y. Wang, C.-Y. Wei, M.-C. Lin, C.-J. Pan, H.-L. Chou, H.-A. Chen, M. Gong, Y. Wu, C. Yuan, M. Angell, Y.-J. Hsieh, Y.-H. Chen, C.-Y. Wen, C.-W. Chen, B.-J. Hwang, C.-C. Chen, H. Dai, *Nat. Commun.* **2017**, *8*, 14283.
- [7] R. J. Gummow, G. Vamvounis, M. B. Kannan, Y. He, *Adv. Mater.* **2018**, *30*, 1801702.
- [8] A. Ponrouch, M. R. Palacín, *Curr. Opin. Electrochem.* **2018**, *9*, 1.
- [9] E. R. Nightingale, *J. Phys. Chem.* **1959**, *63*, 1381.
- [10] S. Gheyhani, Y. Liang, F. Wu, Y. Jing, H. Dong, K. K. Rao, X. Chi, F. Fang, Y. Yao, *Adv. Sci.* **2017**, *4*, 1700465.
- [11] J. Muldoon, C. B. Bucur, T. Gregory, *Chem. Rev.* **2014**, *114*, 11683.
- [12] M. S. Whittingham, *Prog. Solid State Chem.* **1978**, *12*, 41.
- [13] A. L. Lipson, B. Pan, S. H. Lapidus, C. Liao, J. T. Vaughey, B. J. Ingram, *Chem. Mater.* **2015**, *27*, 8442.
- [14] M. Wang, C. Jiang, S. Zhang, X. Song, Y. Tang, H.-M. Cheng, *Nat. Chem.* **2018**, *10*, 667.
- [15] M. Smeu, M. S. Hossain, Z. Wang, V. Timoshevskii, K. H. Bevan, K. Zaghib, *J. Power Sources* **2016**, *306*, 431.
- [16] J. Rogosic, *Ph.D. Thesis*, Massachusetts Institute of Technology, **2014**.
- [17] M. Cabello, F. Nacimiento, J. R. González, G. Ortiz, R. Alcántara, P. Lavela, C. Pérez-Vicente, J. L. Tirado, *Electrochem. Commun.* **2016**, *67*, 59.
- [18] M. E. A. Dompablo, C. Krich, J. Nava-Avendaño, N. Biškup, M. R. Palacín, F. Bardé, *Chem. Mater.* **2016**, *28*, 6886.
- [19] M. Liu, Z. Rong, R. Malik, P. Canepa, A. Jain, G. Ceder, K. A. Persson, *Energy Environ. Sci.* **2015**, *8*, 964.
- [20] M. E. Arroyo-de Dompablo, C. Krich, J. Nava-Avendaño, M. R. Palacín, F. Bardé, *Phys. Chem. Chem. Phys.* **2016**, *18*, 19966.
- [21] D. S. Tchitchekova, A. Ponrouch, R. Verrelli, T. Broux, C. Frontera, A. Sorrentino, F. Bardé, N. Biskup, M. E. Arroyo-de Dompablo, M. R. Palacín, *Chem. Mater.* **2018**, *30*, 847.
- [22] A. L. Lipson, S. Kim, B. Pan, C. Liao, T. T. Fister, B. J. Ingram, *J. Power Sources* **2017**, *369*, 133.
- [23] J. A. Read, A. V. Cresce, M. H. Ervin, K. Xu, *Energy Environ. Sci.* **2014**, *7*, 617.
- [24] J. A. Seel, J. R. Dahn, *J. Electrochem. Soc.* **2000**, *147*, 892.
- [25] D. Billaud, A. Pron, F. L. Vogel, *Synth. Met.* **1980**, *2*, 177.
- [26] N. Emery, C. Hérol, P. Lagrange, *J. Solid State Chem.* **2005**, *178*, 2947.
- [27] D. S. Tchitchekova, D. Monti, P. Johansson, F. Bardé, A. Randon-Vitanova, M. R. Palacín, A. Ponrouch, *J. Electrochem. Soc.* **2017**, *164*, A1384.
- [28] D. Aurbach, R. Skaletsky, Y. Gofer, *J. Electrochem. Soc.* **1991**, *138*, 3536.
- [29] G. G. Amatucci, F. Badway, A. Singhal, B. Beaudoin, G. Skandan, T. Bowmer, I. Plitz, N. Pereira, T. Chapman, R. Jaworski, *J. Electrochem. Soc.* **2001**, *148*, A940.
- [30] T. T. Tran, M. N. Obrovac, *J. Electrochem. Soc.* **2011**, *158*, A1411.
- [31] A. Ponrouch, D. Tchitchekova, C. Frontera, F. Bardé, M. E. A. Dompablo, M. R. Palacín, *Electrochem. Commun.* **2016**, *66*, 75.
- [32] L. M. Vrana, *Kirk-Othmer Encyclopedia of Chemical Technology*, Wiley, Hoboken, NJ **2011**, pp. 1–10.
- [33] A. Palenzona, P. Manfrinetti, M. Fornasini, *J. Alloys Compd.* **2000**, *312*, 165.
- [34] H. Okamoto, *J. Phase Equilib. Diffus.* **2013**, *34*, 171.
- [35] P. Franke, D. Neuschütz, Scientific Group Thermodata Europe, *Binary Systems. Part 5: Binary Systems Supplement 1*, Springer, Berlin **2007**, pp. 1–3.
- [36] K. Kang, Y. S. Meng, J. Bréger, C. P. Grey, G. Ceder, G. Ceder, *Science* **2006**, *311*, 977.
- [37] Z. Yao, S. Kim, M. Aykol, Q. Li, J. Wu, J. He, C. Wolverton, *Chem. Mater.* **2017**, *29*, 9011.
- [38] C. Zhan, Z. Yao, J. Lu, L. Ma, V. A. Maroni, L. Li, E. Lee, E. E. Alp, T. Wu, J. Wen, Y. Ren, C. Johnson, M. M. Thackeray, M. K. Y. Chan, C. Wolverton, K. Amine, *Nat. Energy* **2017**, *2*, 963.
- [39] Q. Li, H. Liu, Z. Yao, J. Cheng, T. Li, Y. Li, C. Wolverton, J. Wu, V. P. Dravid, *ACS Nano* **2016**, *10*, 8788.
- [40] A. Urban, D.-H. Seo, G. Ceder, *NPJ Comput. Mater.* **2016**, *2*, 16002.
- [41] S. Kim, Z. Yao, J.-M. Lim, M. C. Hersam, C. Wolverton, V. P. Dravid, K. He, *Adv. Mater.* **2018**, *30*, 1804925.
- [42] D. Morgan, A. Van der Ven, G. Ceder, *Electrochem. Solid-State Lett.* **2004**, *7*, A30.
- [43] Z. Yao, S. Kim, K. Michel, Y. Zhang, M. Aykol, C. Wolverton, *Phys. Rev. Mater.* **2018**, *2*, 065402.
- [44] H.-C. Yu, C. Ling, J. Bhattacharya, J. C. Thomas, K. Thornton, A. Van der Ven, *Energy Environ. Sci.* **2014**, *7*, 1760.
- [45] Z. Rong, R. Malik, P. Canepa, G. S. Gautam, M. Liu, A. Jain, K. Persson, G. Ceder, *Chem. Mater.* **2015**, *27*, 6016.
- [46] A. Jain, G. Hautier, C. J. Moore, S. P. Ong, C. C. Fischer, T. Mueller, K. A. Persson, G. Ceder, *Comput. Mater. Sci.* **2011**, *50*, 2295.
- [47] Z. Yao, S. Kim, J. He, V. I. Hegde, C. Wolverton, *Sci. Adv.* **2018**, *4*, eaao6754.
- [48] S. Curtarolo, G. L. W. Hart, M. B. Nardelli, N. Mingo, S. Sanvito, O. Levy, *Nat. Mater.* **2013**, *12*, 191.
- [49] M. Amsler, Z. Yao, C. Wolverton, *Chem. Mater.* **2017**, *29*, 9819.
- [50] A. Belsky, M. Hellenbrandt, V. L. Karen, P. Luksch, *Acta Crystallogr., Sect. B: Struct. Sci.* **2002**, *58*, 364.
- [51] S. Kirklin, J. E. Saal, B. Meredig, A. Thompson, J. W. Doak, M. Aykol, S. Rühl, C. Wolverton, *NPJ Comput. Mater.* **2015**, *1*, 15010.
- [52] J. E. Saal, S. Kirklin, M. Aykol, B. Meredig, C. Wolverton, *JOM* **2013**, *65*, 1501.

- [53] L. Y. Beaulieu, K. W. Eberman, R. L. Turner, L. J. Krause, J. R. Dahn, *Electrochem. Solid-State Lett.* **2001**, *4*, A137.
- [54] C. Guminski, *J. Phase Equilib.* **1993**, *14*, 90.
- [55] G. Kresse, J. Hafner, *Phys. Rev. B* **1993**, *47*, 558.
- [56] G. Kresse, J. Hafner, *Phys. Rev. B* **1994**, *49*, 14251.
- [57] G. Kresse, J. Furthmüller, *Comput. Mater. Sci.* **1996**, *6*, 15.
- [58] G. Kresse, *Phys. Rev. B* **1996**, *54*, 11169.
- [59] P. E. Blöchl, *Phys. Rev. B* **1994**, *50*, 17953.
- [60] J. P. Perdew, M. Ernzerhof, K. Burke, *J. Chem. Phys.* **1996**, *105*, 9982.
- [61] M. K. Aydinol, A. F. Kohan, G. Ceder, K. Cho, J. Joannopoulos, *Phys. Rev. B* **1997**, *56*, 1354.
- [62] C. Wolverton, A. Zunger, *Phys. Rev. Lett.* **1998**, *81*, 606.
- [63] H. Liu, Q. Li, Z. Yao, L. Li, Y. Li, C. Wolverton, M. C. Hersam, V. P. Dravid, *Adv. Mater.* **2018**, *30*, 1704851.
- [64] Q. Li, J. Wu, Z. Yao, M. M. Thackeray, C. Wolverton, V. P. Dravid, *Nano Energy* **2018**, *44*, 15.